8674 *Inorg. Chem.* **2010**, *49*, 8674–8683
DOI: 10.1021/ic9024316

Inorganic Chemistry
Article

Simple Shape-Controlled Synthesis of Carbon Hollow Structures

Mingtao Zheng, Yingliang Liu,* Shuai Zhao, Wenqi He, Yong Xiao, and Dingsheng Yuan

Department of Chemistry and Institute of Nanochemistry, Jinan University, Guangzhou 510632, People's Republic of China

Received December 7, 2009

This study reports a simple method for the controlled synthesis of uniformly shaped carbon hollow structures by an ethanol-assisted thermolysis of zinc acetate. The experimental evidence reveals that the generated zinc oxide nanostructures act as in-situ templates to form the carbon hollow structures. The morphologies, including the shell thickness, cavity size, and aspect ratio, can be controlled by the reaction time and the heating procedure, and hollow nanospheres, nanocapsules, nanorods, and microtubes can be obtained. Experimental results show that the as-synthesized carbon hollow structures exhibit excellent thermal and structural stability to temperatures as high as 1200 °C.

Introduction

In recent years, hollow micro- and nanoscale materials are of particular interest due to their distinctive functions, novel properties, and potential applications in advanced devices and biotechnologies.[1] Among them, carbon hollow structures, such as hollow spheres and capsules, have attracted growing research interest owing to their excellent properties such as low density, high specific surface area, high damping characteristics, good chemical stability, and available hollow interiors,[2] which make them technologically important in a wide rang of potential applications in lithium-ion batteries,[3] catalysis supports,[4] supercapacitors,[5] hydrogen storage,[6] drug delivery,[7] etc. This promise has motivated intense research efforts seeking to develop special and general routes for carbon hollow structure synthesis. Templating against colloidal particles is probably the most effective and general method for preparing carbon hollow structures.[8] Monodisperse latex and silica spheres are usually used as colloidal templates because they are readily available in a wide range of sizes and morphologies. The synthesis procedure commonly involves three steps: introduction of the carbon precursor on the template by liquid impregnation or by gas-phase chemical vapor deposition; carbonization of the carbon precursor (usually at high temperature); and finally removal of the colloidal template.[9] The apparent advantage of the template method is that the shape and cavity size of the obtained hollow structures are directly governed by the template. However, removable, expensive polymer latex, silica, or other colloidal particles are energy-consuming and uneconomic, and the synthesis procedure is complicated and time-consuming. In particular, to acquire hollow spheres with uniform shell thickness, prior surface functionalization or modification before the coating step is often required.

Other template-free routes, including solvothermal method and direct chemical reaction, have been developed for the preparation of carbon hollow structures.[10] Wu and co-workers, for example, have successfully prepared necklace-like hollow carbon nanospheres using $Fe(C_5H_5)_2$ and C_5Cl_6 as starting materials.[6] However, the obtained carbon hollow spheres by these methods presented a wide particle size distribution, and the precursors or reducing agents were often expensive and poisonous. Therefore, it is highly desirable to explore other

*To whom correspondence should be addressed. E-mail: tliuyl@jnu.edu.cn.

(1) (a) Zhong, Z.; Yin, Y.; Gates, B.; Xia, Y. *Adv. Mater.* **2000**, *12*, 206–209. (b) Caruso, F. *Adv. Mater.* **2001**, *13*, 11–22. (c) Caruso, F. *Top. Curr. Chem.* **2003**, *227*, 145–168. (d) Xu, X. L.; Asher, S. A. *J. Am. Chem. Soc.* **2004**, *126*, 7940–7945. (e) Zhan, J.; Bando, Y.; Hu, J.; Yin, L.; Yuan, X.; Sekiguchi, T.; Golberg, D. *Angew. Chem., Int. Ed.* **2006**, *45*, 228–231. (f) Miao, J. J.; Jiang, L. P.; Liu, C.; Zhu, J. M.; Zhu, J. J. *Inorg. Chem.* **2007**, *46*, 5673–5677. (g) Zhao, Y.; Jiang, L. *Adv. Mater.* **2009**, *21*, 3621–3638.

(2) (a) Li, L. C.; Song, H. H.; Chen, X. H. *Carbon* **2006**, *44*, 596–599. (b) Zhang, J.; Perez, R. J.; Lavernia, E. J. *J. Mater. Sci.* **1993**, *28*, 2395–2404. (c) Bokros, J. C. *Carbon* **1977**, *15*, 353–371.

(3) (a) Lee, K. T.; Jung, Y. S.; Oh, S. M. *J. Am. Chem. Soc.* **2003**, *125*, 5652–5653. (b) Wang, Y.; Su, F.; Lee, J. Y.; Zhao, X. S. *Chem. Mater.* **2006**, *18*, 1347–1353. (c) Zhang, W.; Hu, J.; Guo, Y.; Zheng, S.; Zhong, L.; Song, W.; Wan, L. *Adv. Mater.* **2008**, *20*, 1160–1165.

(4) (a) Teng, S. J.; Wang, X. X.; Xia, B. Y.; Wang, J. N. *J. Power Sources* **2010**, *195*, 1065–1070. (b) Ng, Y. H.; Ikeda, S.; Harada, T.; Higashida, S.; Sakata, T.; Mori, H.; Matsumura, M. *Adv. Mater.* **2007**, *19*, 597–601. (c) Song, Y. Y.; Li, Y.; Xia, X. H. *Electrochem. Commun.* **2007**, *9*, 201–205. (d) Wen, Z.; Wang, Q.; Zhang, Q.; Li, J. *Electrochem. Commun.* **2007**, *9*, 1867–1872.

(5) Zhang, F. B.; Li, H. L. *Mater. Chem. Phys.* **2006**, *98*, 456–458.

(6) Wu, C.; Zhu, X.; Ye, L.; Ouyang, C.; Hu, S.; Lei, L.; Xie, Y. *Inorg. Chem.* **2006**, *45*, 8543–8550.

(7) Liu, B. Y.; Jia, D. C.; Rao, J. C.; Meng, Q.; Shao, Y. *Bull. Mater. Sci.* **2008**, *31*, 771–774.

(8) (a) Chang-Chien, C. Y.; Hsu, C. H.; Lee, T. Y.; Liu, C. W.; Wu, S. H.; Lin, H. P.; Tang, C. Y.; Lin, C. Y. *Eur. J. Inorg. Chem.* **2007**, 3798–3804. (b) Li, F.; Zou, Q.; Xia, Y. *J. Power Sources* **2008**, *177*, 546–552. (c) Yoon, S. B.; Sohn, K.; Kim, J. Y.; Shin, C. H.; Yu, J. S.; Hyeon, T. *Adv. Mater.* **2002**, *14*, 19–21. (d) Kim, M.; Sohn, K.; Na, H. B.; Hyeon, T. *Nano Lett.* **2002**, *2*, 1383–1387. (e) Geng, B. Y.; Ma, J. Z.; Du, Q. B.; Liu, X. W.; Zhang, L. D. *Mater. Sci. Eng., A* **2007**, *466*, 96–100. (f) Song, Y. Y.; Li, Y.; Xia, X. H. *Electrochem. Commun.* **2007**, *9*, 201–205.

(9) Xia, Y.; Mokaya, R. *Adv. Mater.* **2004**, *16*, 886–891.

Published on Web 08/30/2010

simpler and more efficient strategies for carbon hollow structure synthesis. Furthermore, large-scale synthesis of carbon hollow structures from a simple, controllable method and cost-effective precursors is still a critical target in scientific and industrial research.

In recent years, an in-situ template method has been widely used to fabricate nanoparticles with a hollow interior structure.[11] This template approach is much simpler than conventional ones involving separate procedures for preparation of template materials and suitable for large-scale production. Hence it offers an attractive method for the preparation of hollow structures with different morphologies, including silica, metal oxides, selenides, chalcogenides, sulfates, and polyphosphazenes.[11,12] In-situ template synthesis of carbon materials, such as mesoporous carbons and nanocages, has also been reported.[13] More recently, solid-state pyrolysis of organometallic precursors has emerged as an alternative method for preparing carbon nanostructures such as carbon nanotubes, onions, and capsules.[14] In such a process, the organometallic compounds can serve as a dual source of both the carbon and the metal catalyst nanoparticles, and the pyrolysis is carried out not in the gas phase but in the solid state at "low" temperature. Our recent research work on the synthesis of carbon materials has shown that the ethanol-assisted thermolysis of metal acetates could obtain carbon micro- and nanostructures with novel morphologies, such as flower-like microstructures and two-layer planes by thermolysis of magnesium acetate in ethanol in a stainless autoclave system[15] and Z-shaped carbon nanotubes in the absence of ethanol.[16] In this report, we combine this experimentally simple method with the use of inexpensive precursors to fabricate carbon hollow structures through the ethanol-assisted thermolysis of zinc acetate ($Zn(Ac)_2$) in a sealed autoclave system. During the process, the zinc oxide (ZnO) nanoparticles, which are generated from the decomposition of zinc carbonate ($ZnCO_3$) resulting from the decomposition of $Zn(Ac)_2$ formed in situ initially, act as in-situ templates to form the carbon hollow structures. Remarkably, the morphology including the shell thickness, cavity size, and aspect ratio of the hollow structures can be controlled by the reaction time and the heating procedure.

Experimental Section

Synthesis of Carbon Hollow Spheres. All chemicals were analytical and used as received without further purification. In a typical procedure, 4 g of $Zn(Ac)_2$ was magnetically stirred in 40 mL of absolute ethanol at room temperature for 3 h to form a homogeneous solution. The solution was then placed and sealed into a steel-stainless autoclave with a 50 mL capacity. Subsequently, the autoclave was put into an electronic furnace, which was then heated to 600 °C with a rapid heating rate of 10 °C min^{-1} and maintained at this temperature for 3−12 h. After the autoclave was cooled to room temperature naturally, the dark precipitates were collected and washed with aqueous HCl (1 M), distilled water, and absolute ethanol several times. The product was dried in a vacuum at 60 °C for 6 h.

Synthesis of Carbon Nanocapsules, Hollow Nanorods, and Microtubes. A 4 g amount of $Zn(Ac)_2$ was magnetically stirred in 40 mL of absolute ethanol at room temperature for 3 h. The obtained solution was then sealed into a 50 mL steel-stainless autoclave. The autoclave was first heated to 400 °C, kept at this temperature for different times (1−6 h), then heated slowly to 600 °C over 2 h, and maintained at this temperature for 12 h. After cooling to room temperature, the black products were washed with aqueous HCl (1 M), distilled water, and absolute ethanol several times. All the obtained samples were vacuum-dried at 60 °C for 6 h.

Characterization. Powder XRD patterns were recorded on a MSAL-XD2 X-ray diffractometer with Cu Kα radiation (36 kV, 20 mA, λ = 1.54051 Å). FT-IR spectra were measured by an Equinox 55 (Bruker) spectrometer with the KBr pellet technique ranging from 500 to 4000 cm^{-1}. The Raman spectrum was recorded at room temperature on a Renishaw RM2000 Raman microspectrometer with the 514.5 nm line of an argon laser. The SEM measurements were taken with a Philips XL-30 scanning electron microscope. TEM images and the elements of the products were obtained using a Philips Tecnai-10 and JEOL JEM-2010 transmission electron microscope with an operating voltage of 200 kV. The specific surface areas were determined from nitrogen adsorption using the BET (Brunauer−Emmett−Teller) equation. The total pore volume was determined from the amount of gas adsorbed at the relative pressure of 0.99. Micropore (pore size $<$ 2 nm) volume of the hollow spheres was calculated from the analysis of the absorption isotherm using the HK (Horvath−Kawzoe) method. Pore size distribution (PSD) was derived from the analysis of the adsorption branch using the BJH (Barrett−Joyner−Halenda) method. The gas chromatography and mass spectrometry (GC−MS) technique was performed on the Trace GC−MS. The conditions for GC−MS were given as follows: capillary column: Wax-10 (length: 30 m, diameter: 0.25 mm), injector temperature: 260 °C; column temperature: 80 °C (1 min), 80 → 260 °C (heating rate of 4 °C min^{-1}), 260 °C (10 min); carrier gas: helium, flow rate: 1.2 mL min^{-1}; ionization mode: electronic ionization; electronic bombardment energy: 70 eV, scanning time: 0.5 s, scanning range: 30−500 u. The structure of the compounds was determined by the computer software from the characterized GC−MS graphs.

(10) (a) Li, M.; Wu, Q.; Wen, M.; Shi, J. *Nanoscale Res. Lett.* **2009**, *4*, 1065–1070. (b) Li, G.; Guo, C.; Sun, C.; Ju, Z.; Yang, L.; Xu, L.; Qian, Y. *J. Phys. Chem. C* **2008**, *112*, 1896–1900. (c) Sun, X.; Li, Y. J. *Colloid Interface Sci.* **2005**, *291*, 7–12. (d) Xu, L.; Zhang, W.; Yang, Q.; Ding, Y.; Yu, W.; Qian, Y. *Carbon* **2005**, *43*, 1090–1092. (e) Ni, Y.; Shao, M.; Tong, Y.; Qian, G.; Wei, X. *J. Solid State Chem.* **2005**, *178*, 908–911. (f) Shi, L; Gu, Y.; Chen, L.; Yang, Z.; Ma, J.; Qian, Y. *Chem. Lett.* **2004**, *33*, 532–533. (g) Liu, J.; Shao, M.; Tang, Q. *Carbon* **2003**, *41*, 1682–1685. (h) Xiong, Y.; Xie, Y.; Li, Z.; Wu, C.; Wu, C.; Zhang, R. *Chem. Commun.* **2003**, *7*, 904–905. (i) Hu, G.; Ma, D.; Cheng, M.; Liu, L.; Bao, X. *Chem. Commun.* **2002**, *17*, 1948–1949.

(11) (a) Wang, L.; Tang, F.; Ozawa, K.; Chen, Z. G.; Nukherj, A.; Zhu, Y.; Zou, J.; Cheng, H. M.; Lu, G. Q. *Angew. Chem., Int. Ed.* **2009**, *48*, 7048–7051. (b) Shen, G.; Bando, Y.; Golberg, D. *J. Phys. Chem. B* **2006**, *110*, 23170–23174. (c) Zhu, J. J.; Xu, S.; Wang, H.; Zhu, J. M.; Chen, H. Y. *Adv. Mater.* **2003**, *15*, 156–159.

(12) (a) Xu, H.; Wang, W.; Zhu, W. *Mater. Lett.* **2006**, *60*, 2203–2206. (b) Zhao, J.; Wang, X.; Sun, T.; Li, L. *Nanotechnology* **2005**, *16*, 2450–2454. (c) Zhao, X.; Yu, J.; Tang, H.; Lin, J. J. *Colloid Interface Sci.* **2007**, *311*, 89–93. (d) Kim, B. S.; Lee, K. T.; Huh, P. H.; Lee, D. H.; Jo, N. J.; Lee, J. O. *Synth. Met.* **2009**, *159*, 1369–1372. (e) Fu, J.; Huang, X.; Zhu, Y.; Zhu, L.; Tang, X. *Macromol. Chem. Phys.* **2008**, *209*, 1845–1850. (f) Fu, J.; Huang, X.; Zhu, Y.; Huang, Y.; Tang, X. *Scr. Mater.* **2008**, *58*, 1047–1049. (g) Fu, J.; Huang, X.; Zhu, Y.; Zhu, L.; Tang, X. *Appl. Surf. Sci.* **2009**, *255*, 5088–5091.

(13) (a) Yuan, D.; Zeng, J.; Chen, J.; Liu, Y. *Int. J. Electrochem. Sci.* **2009**, *4*, 562–570. (b) Wang, J. N.; Zhang, L.; Niu, J. J.; Sheng, Z. M.; Zhao, Y. Z.; Chang, H.; Pak, C. *Chem. Mater.* **2007**, *19*, 453–459. (c) Zhang, L.; Wang, J. N.; Niu, J. J. *J. Mater. Sci.* **2007**, *42*, 3692–3694. (d) Ye., J. C.; Sheng, Z. M.; Wang, J. N. *Microporous Mesorporous Mater.* **2006**, *94*, 122–126. (e) Shen, G.; Bando, Y.; Zhi, C.; Golberg, D. *J. Phys. Chem. B* **2006**, *110*, 10714–10719.

(14) (a) Rao, C. N. R.; Govindaraj, A. *Acc. Chem. Res.* **2002**, *35*, 998–1007. (b) Lyer, V. S.; Vollhardt, K. P. C.; Wilhelm, R. *Angew. Chem., Int. Ed.* **2003**, *42*, 4379–4383. (c) Dosa, P. I.; Erben, C.; Lyer, V. S.; Vollhardt, K. P. C.; Wasser, I. M. *J. Am. Chem. Soc.* **1999**, *121*, 10430–10431. (d) Laskoski, M.; Steffen, W.; Morton, J. G. M.; Smith, M. D.; Bunz, U. H. F. *J. Am. Chem. Soc.* **2002**, *124*, 13814–13818. (e) Jain, D.; Winkel, A.; Wilhelm, R. *Small* **2006**, *2*, 752–755.

(15) (a) Xiao, Y.; Liu, Y.; Yuan, D.; Zhang, J.; Gu, Y.; Sun, G. *Carbon* **2006**, *44*, 1589–1591. (b) Xiao, Y.; Liu, Y.; Yuan, D. *Carbon* **2008**, 559–561.

(16) Yuan, D.; Liu, Y.; Xiao, Y.; Cheng, L. *Mater. Chem. Phys.* **2008**, *112*, 27–30.

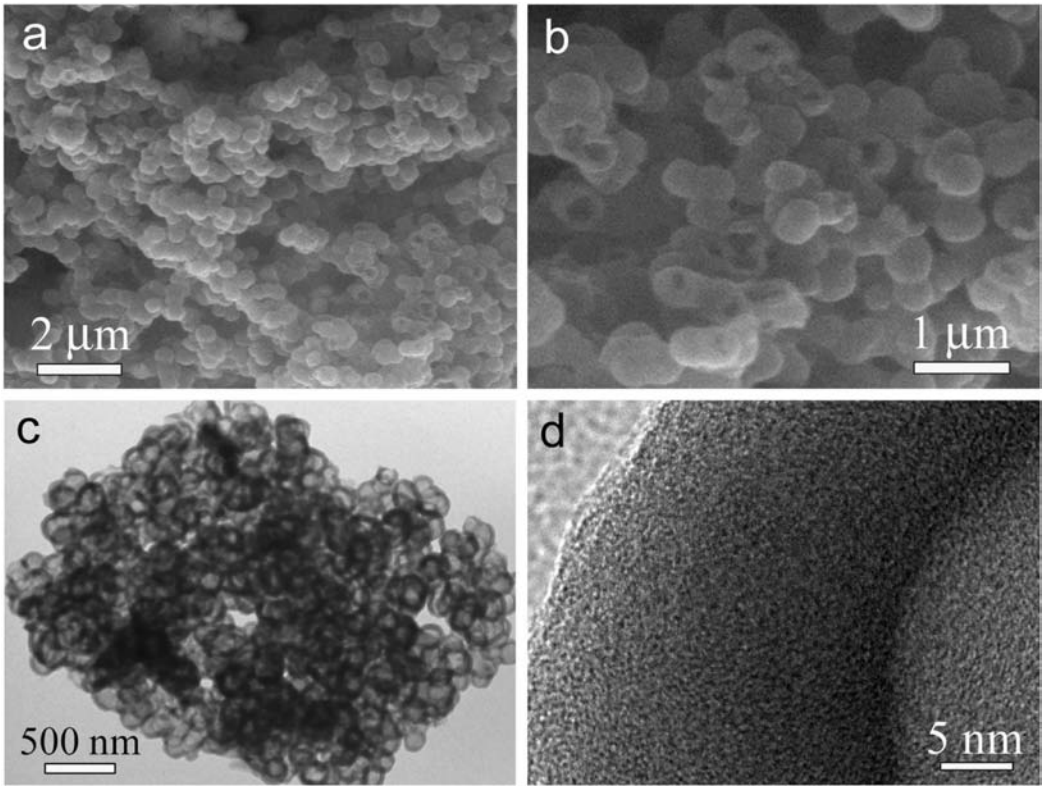

Figure 1. SEM and TEM images of the obtained products after HCl etching by ethanol-assisted pyrolysis of zinc acetate at 600 °C for 12 h: (a) SEM of the sample at low magnification, (b) magnified SEM image shows some broken nanospheres, (c) TEM image, and (d) detail from the disordered carbon shell of the hollow spheres.

Results and Discussion

Structure and Morphology of Carbon Hollow Nanospheres. Scanning electron microscopy (SEM), transmission electron microscopy (TEM), and high-resolution TEM (HRTEM) were employed to observe the structure and morphology of the samples. Representative images of the morphology of the HCl-etched samples, which were prepared by ethanol-assisted thermolysis of $Zn(Ac)_2$ at 600 °C for 12 h, are shown in Figure 1. The SEM images (Figure 1a and b) reveal that the samples contained a large number of nanospheres with outer diameter of about 300−400 nm. Compared to other related references reported previously, this dimensionality dispersity of the carbon hollow spheres is similar to those prepared by template methods,[8,9] while is better than those synthesized by other template-free routes.[6,10,14] It can also be seen from Figure 1b that there are some broken nanospheres, indicating the hollow structure of the nanospheres. The low-resolution TEM image (Figure 1c) shows the nanospheres present as lighter contrast in the center, indicating the hollow structures with cavity size varying from 130 to 200 nm. The darker contrast of the rims would correspond to the shells of the nanospheres, the thickness of these walls being around 40−50 nm. The HRTEM image from such a hollow nanosphere, Figure 1d, illustrates that the carbon shells consist of either amorphous or disordered carbon, without the presence of graphitic layers due to the "low" carbonization temperature.

The Raman spectrum was also used to further analyze the molecular structure of the hollow spheres. Figure 2a shows the micro-Raman spectrum of the sample obtained from the ethanol-assisted thermolysis of $Zn(Ac)_2$ at 600 °C for 12 h. Two broad peaks can be observed. One bond is located around 1340 cm^{-1} (D-band; the defects within the carbon) and the other is around 1580 cm^{-1} (G-band; the interplane sp^2 C−C stretching), which also indicate the amorphous carbon structure. It is known that the graphitization degree of carbons can be confirmed by the width of the I_G peak and the value of I_D/I_G. The relatively large I_D/I_G (about 0.75) indicated the lower graphitization degree in the resultant hollow carbon spheres, which is well consistent with the HRTEM observation. These results show that the hollow carbon spheres obtained by this method are amorphous carbons.

The porosity of the obtained hollow carbon spheres was investigated by nitrogen adsorption−desorption isotherms (Figure 2b). The pore size was estimated from the PSD maximum as 1.9 nm (Figure 2c). The hollow spheres exhibited a high surface area of 371 $m^2\ g^{-1}$ (micropore area: 274 $m^2\ g^{-1}$; external surface area: 97 $m^2\ g^{-1}$) and a total pore volume of 0.19 $cm^3\ g^{-1}$, which are mainly attributable to the presence of the nanopores in the shell (micropore volume: 0.13 $cm^3\ g^{-1}$). The presence of nanopores in the shells allows the etching agent to come into the interior, and thus the cores can be removed. The micropore area of hollow carbon spheres is much larger than the external surface area, which makes the hollow carbon spheres an ideal candidate for hydrogen storage.

Thermolysis Process of $Zn(Ac)_2$ and Carbon Precursors. The phase evolution was investigated by powder X-ray diffraction (XRD) examination. A series of evolutional XRD patterns of the samples obtained at different thermolysis

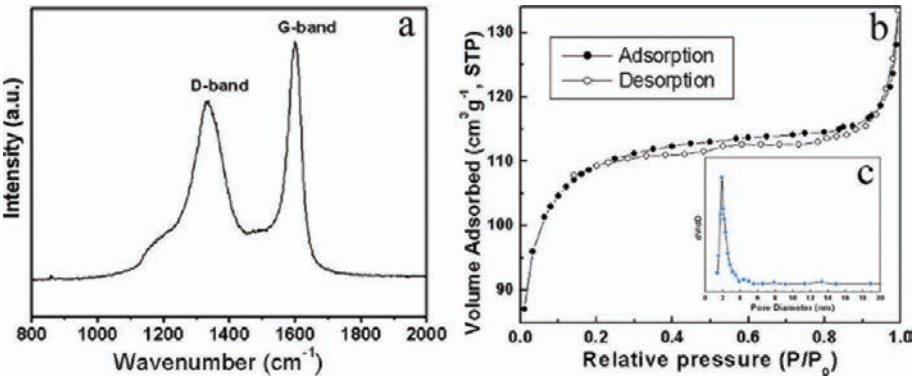

Figure 2. Raman spectrum (a), adsorption−desorption isotherms (b), and pore size distribution (c) of the as-prepared carbon hollow spheres.

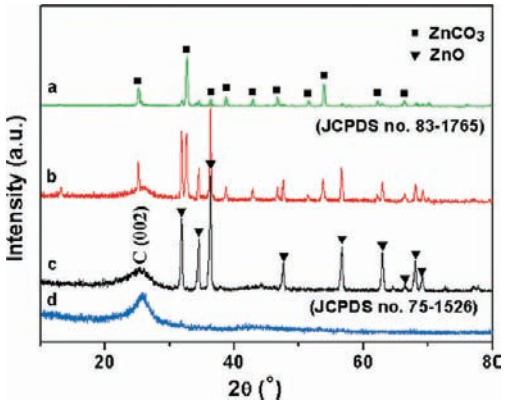

Figure 3. XRD patterns of the samples before HCl etching obtained by ethanol-assisted thermolysis of $Zn(Ac)_2$ at different reaction temperatures for 12 h: (a) 400 °C, (b) 500 °C, and (c) 600 °C. (d) XRD pattern of the product obtained after HCl etching of the sample c.

temperatures are shown in Figure 3. The solid products formed at 400 °C are phase-pure rhomb-centered $ZnCO_3$ (JCPDS no. 83-1765), and no carbon peaks are observed, while the coexistence of $ZnCO_3$ and ZnO in the products obtained at a temperature of 500 °C can be clearly observed (Figure 3b). When the reaction temperature increases up to 600 °C, the $ZnCO_3$ is decomposed completely, and pure hexagonal-phase ZnO can be obtained (Figure 3c, JCPDS no. 75-1526). As shown in Figure 3b and c, the broad diffraction peaks at a 2θ of about 25° are well assigned to amorphous carbons, which are in good agreement with the HRTEM and Raman results.

According to the above XRD results, the thermolysis pathway of $Zn(Ac)_2$ and carbon precursors during this process can be illustrated as follows:

$$CH_3COOZnOOCCH_3 \xrightarrow{\text{ethanol}} ZnCO_3 + CH_3COCH_3 \quad (1)$$

$$ZnCO_3 \rightarrow ZnO + CO_2 \quad (2)$$

$$m CH_3COCH_3 + n CH_3CH_2OH \xrightarrow{ZnO} ZnO@C \text{ structures} + (2m+n)H_2 + (m+n)H_2O \quad (3)$$

As shown in eq 1, the ethanol-assisted thermolysis of $Zn(Ac)_2$ results in the formation of $ZnCO_3$ nanoparticles in the initial stage. This process is different from the solid-state pyrolysis of organometallic precursors reported previously, in which the pyrolysis of organometallic compounds often leads to the formation of metallic nanoparticles.[14] This is also different from the decomposition of cobalt acetate in absolute ethanol in the presence of sodium fluoride or chloride, where cubic cobalt nanoskeletons or spheres are formed.[17] With the increase of the reaction temperature, the generated $ZnCO_3$ is then decomposed in situ to produce ZnO nanostructures (eq 2). It is noteworthy that the morphology of the $ZnCO_3$ nanoparticles can be well inherited by ZnO; that is, the decomposition of $ZnCO_3$ does not lead to a change in the morphology. At the same time, the in-situ carbonization of organic precursors resulted in the formation of carbon, which was deposited onto the surfaces of the ZnO nanoparticles; thus, ZnO@C core/shell structures were formed (eq 3). It is also worth noting that the decomposition of $ZnCO_3$ nanocrystals and the carbonization of carbon precursors is a synchronous process at high temperature. Therefore $ZnCO_3$/ZnO@C core/shell structures were obtained indeed at a temperature of 500 °C (Figure 3b).

The core/shell structures are clearly revealed by the TEM images in Figure 4a and the inset. It is apparent that ZnO cores are completely encapsulated in the carbon shells. The size of these cores is about 120−160 nm and the shell thickness is about 40 nm, which is well consistent with the cavity size and shell thickness of the hollow spheres (Figure 1c). Figure 4b represents a HRTEM image of such a core/shell structure, showing the wall structure and the material inside the capsule. The selected area electron diffraction (SAED) pattern taken from such a filled capsule clearly shows the single-crystal-like structure of the core material (the inset in Figure 4b). The element composition is further confirmed with energy dispersive X-ray spectroscopy (EDS) analysis. The spectrum, taken from the center area of a core/shell particle, shows strong Zn, C, and O signals (Figure 5a). After etching by aqueous HCl, the EDS spectrum denotes the presence of carbon, and no Zn signal can be observed, indicating that the ZnO core has been completely eliminated (Figure 5b). These results indicate that ZnO generated in situ resulting from the decomposition of $ZnCO_3$

(17) (a) Wang, X.; Fu, H.; Peng, A.; Zhai, T.; Ma, Y.; Yuan, F.; Yao, J. *Adv. Mater.* **2009**, *21*, 1636–1640. (b) Wang, X.; Yuan, F.; Hu, P.; Yu, L.; Bai, L. *J. Phys. Chem. C* **2008**, *112*, 8773–8778.

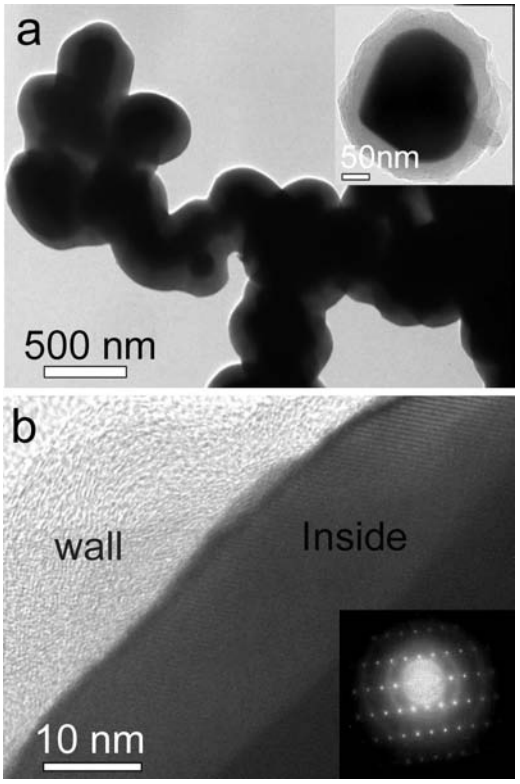

Figure 4. (a) TEM image of ZnO@C core/shell structures and (b) HRTEM image of a capsule wall and the materials contained inside the nanocapsule.

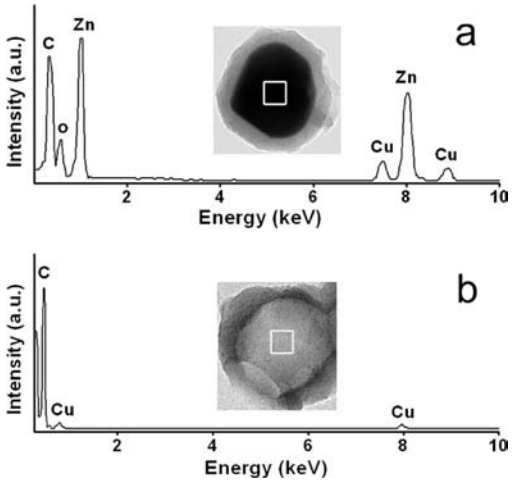

Figure 5. EDS spectra of the obtained products before (a) and after (b) removal of ZnO cores by HCl etching.

acts as template for the formation of the carbon hollow spheres.

Effect of the Reaction Time on the Morphology of the Carbon Hollow Structures. It is well known that the shell thickness and cavity size are the two most important parameters that determine the mechanical and adsorption properties of the hollow structures.[18] For example, hollow spheres with a tunable cavity size can be very useful in the study of physical phenomena as well as in practical applications.[19] The previous experiments that related to the template synthesis of capsules with controllable cavity size were often achieved by the preparation of colloidal template particles with desired size, while, in the present work, the shell thickness and cavity size can be controlled only by tuning the reaction time. Figure 6 shows the TEM images of the samples prepared by the ethanol-assisted thermolysis of zinc acetate at 600 °C for different reaction times. In a short reaction of 3 h, carbon nanocapsules with a shell thickness of about 15 nm can be obtained, as shown in Figure 6a. It is noticeable that the resultant nanocapsules at this stage appear to be incompletely encapsulated, resulting in the formation of a large number of broken nanocapsules (Figure S1, Supporting Information). As the time increases (6−48 h), carbon nanocapsules with shell thicknesses from 20 to 70 nm are obtained. It can also be observed from Figure 6 that the cavity size increases from 80 to 600 nm with the increase of reaction time, indicating that $ZnCO_3$ nanoparticles produced from the decomposition of $Zn(Ac)_2$ in this sealed autoclave system prefer to form larger nanoparticles at longer reaction time. According to the above analysis of the thermolysis process, the growth and decomposition of $ZnCO_3$ nanocrystals and the carbonization of carbon precursors is a synchronous process at high temperature; that is, the growth of $ZnCO_3$ nanocrystals would not be terminated until the decomposition of $ZnCO_3$ was completed even at high temperatures of 500−600 °C. The diameter of $ZnCO_3$ particles increases with the increase of the pyrolysis time, and hence the size of the produced ZnO particles increases. Therefore both shell thickness and cavity size of the obtained carbon hollow spheres increase with pyrolysis time. It is interesting to note that some polyhedral nanocapsules can also be observed, besides the spherical particles, as shown in Figure 6c and d.

Effect of the Heating Procedure on the Morphology of the Carbon Hollow Structures. It is clear from the above results that ZnO nanoparticles resulting from the decomposition of $ZnCO_3$, which was formed in situ from the pyrolysis of $Zn(Ac)_2$ initially, act as an in-situ template to form the carbon hollow spheres. Thus, it is reasonable to assume that carbon hollow structures with controllable morphology can be achieved by controlling the morphology of the $ZnCO_3$ nanoparticles since the in-situ decomposition of $ZnCO_3$ to produce ZnO does not result in a change in morphology. Interestingly, our experiments show that the controlled synthesis of carbon hollow structures with novel morphology can be realized easily by tuning the simple heating process with different thermal gradients. Figure 7 shows the SEM and TEM images of the samples obtained by a designed ethanol-assisted thermolysis of $Zn(Ac)_2$. Maintaining at 400 °C for different times and then heating to 600 °C for 12 h results in the formation of carbon hollow structures with different morphologies and aspect ratios, where the aspect ratio of 1 corresponds to spherical particles. In a short reaction time of 1 h at low temperature (400 °C), carbon nanocapsules with an aspect ratio of about 1.5 are obtained (Figure 7a and b). As that time increases (2−3 h), a large

(18) (a) Zhang, Y. S.; Xu, W. H.; Yao, W. T.; Yu, S. H. *J Phys. Chem. C* **2009**, *113*, 8588–8594. (b) Lou, X. W.; Archer, L. A.; Yang, Z. *Adv. Mater.* **2008**, *20*, 1–33. (c) Yang, Z.; Niu, Z.; Lu, Y.; Hu, Z.; Han, C. C. *Angew. Chem., Int. Ed.* **2003**, *42*, 1943–1945.

(19) Peng, S.; Sun, S. *Angew. Chem., Int. Ed.* **2007**, *46*, 4155–4158.

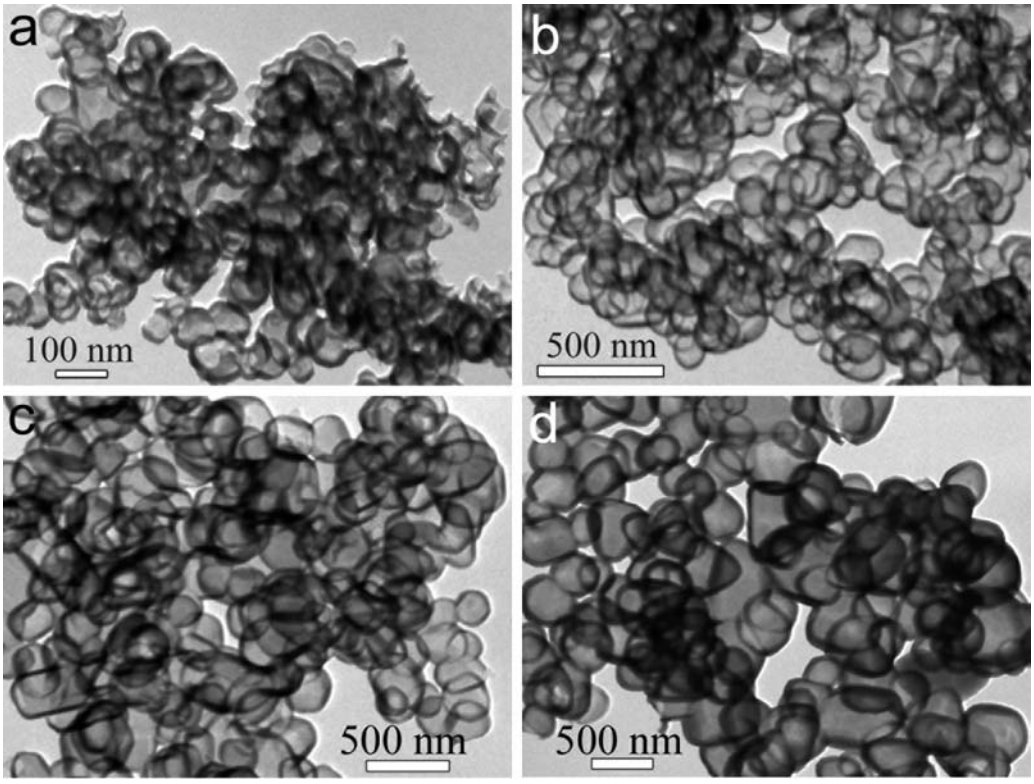

Figure 6. TEM images of carbon nanocapsules prepared by ethanol-assisted thermolysis of $Zn(Ac)_2$ at 600 °C for different times: (a) 3 h, (b) 6 h, (c) 24 h, and (d) 48 h.

amount of hollow nanorods with an average diameter of about 300 nm, a length varying from 800 nm to 1 μm, and an aspect ratio of about 3 can be achieved (Figure 7c and d). Extending the thermolysis time to 6 h at 400 °C dramatically improves the formation of micrometer-sized carbon tubes (Figure 7e and f). Similar to the spherical counterparts, corresponding ZnO@C core/shell intermediate structures are obtained before HCl etching (Figure S2, Supporting Information), indicating that these novel carbon hollow structures are also formed by in-situ templates of ZnO nanoparticles. These results demonstrate that maintaining the thermolysis at low temperature (400 °C) for a certain time plays an important role in the formation of novel ZnO@C core/shell structures and the final hollow carbon structures. This finding is not surprising, since changing the heating process affects the conditions of decomposition of $Zn(Ac)_2$ and the growth of $ZnCO_3$ nanoparticles.

To further investigate the formation process of these novel carbon hollow structures, controlled experiments were performed at 400 °C for different reaction times. Consequently, only $ZnCO_3$ nanoparticles were obtained. SEM images of the samples obtained by ethanol-assisted thermolysis of $Zn(Ac)_2$ for reaction time of 3−12 h are shown in Figure 8. It can be seen that the length, diameter, and aspect ratio of the $ZnCO_3$ nanoparticles increase with the increase of reaction time. In a short reaction time (3 h), spherical nanoparticles with a size of 300−400 nm can be obtained (Figure 8a). Prolonging the reaction to 6 h, short nanorods with an average diameter of 400 nm and length of 800−900 nm are observed in the products (Figure 8b). When the reaction time is extended to 12 h, micrometer-sized rods with a diameter of about 800 nm and length up to 10 μm are obtained (Figure 8c). These results suggest that the carbon hollow structures are formed by the in-situ carbonization of carbon precursors on the surface of the in-situ-generated ZnO nanoparticles resulting from the decomposition of $ZnCO_3$ nanostructures, which are either nanospheres or nanorods with different aspect ratios.

Roles of Ethanol on the Formation of Carbon Hollow Structures. It was found that, in the absence of ethanol, the thermolysis of $Zn(Ac)_2$ at 600 °C for 12 h resulted in the formation of large aggregations with hollow interiors, and no carbon nanospheres or capsules could be obtained (Figure S3, Supporting Information). On the other hand, when ethanol was displaced by other alcohols (e.g., glycol) in the synthesis, relatively uniform carbon nanocapsules could also be obtained (Figure S4, Supporting Information). These results indicate that the ethanol plays a crucial role in the formation of these carbon hollow structures including hollow nanospheres, nanocapsules, nanorods, and microtubes.

With increasing reaction temperature, ethanol is polymerized into organic compounds, such as ethers, esters, or other oligomers. It is noteworthy that the components of these oligomers in the liquid fractions are very complicated and are difficult to fully characterize by a single analytical technique. The GC−MS technique, which is a powerful tool to identify the components of the complicated thermolysis products of the biomass,[20] is employed to characterize the typical compounds in the liquid

(20) (a) Shen, D. K.; Gu, S. *Bioresour. Technol.* **2009**, *100*, 6496–6504. (b) Yip, J.; Chen, M.; Szeto, Y. S.; Yan, S. *Bioresour. Technol.* **2009**, *100*, 6674–6678.

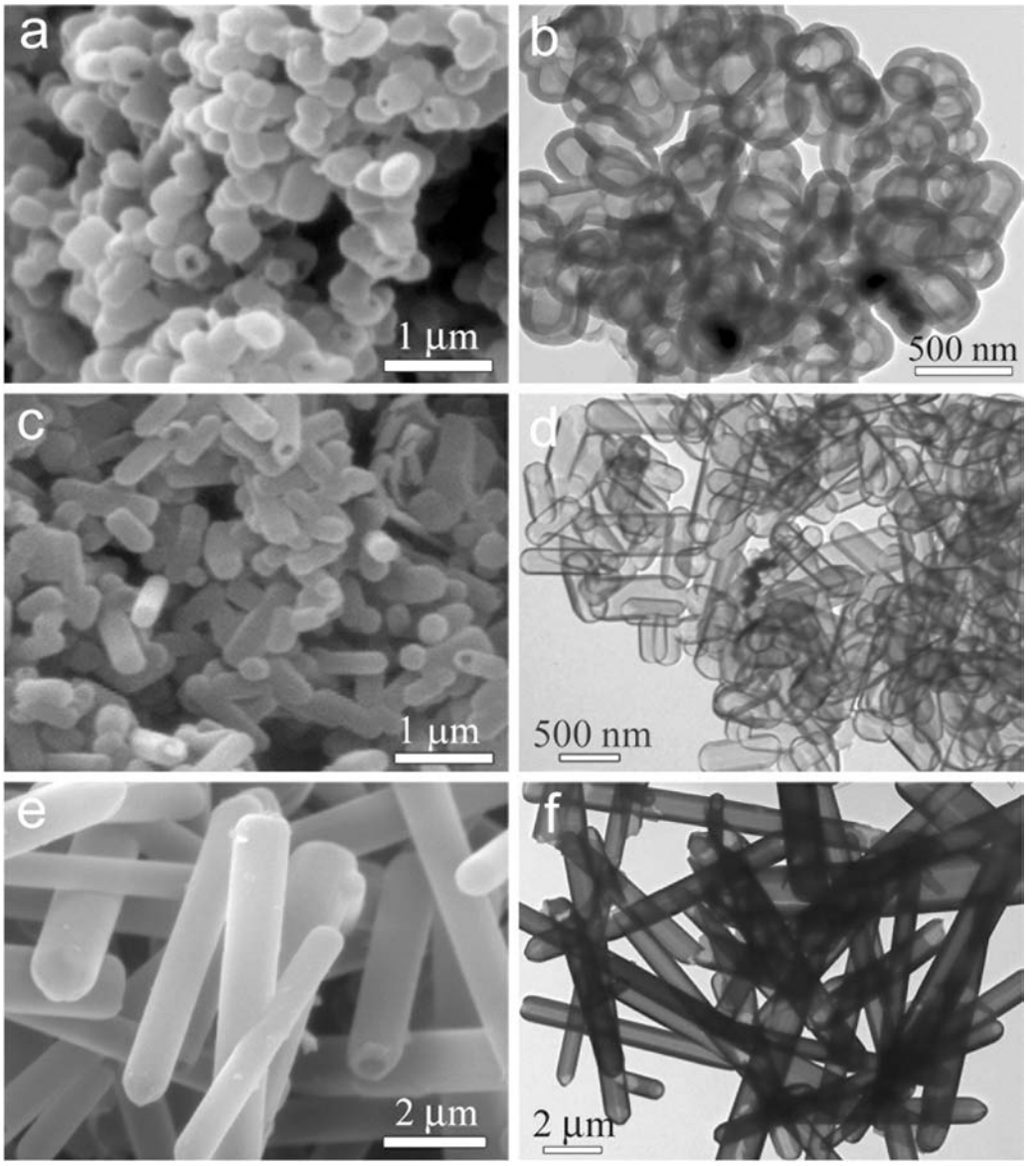

Figure 7. SEM and TEM images of the samples obtained by ethanol-assisted thermolysis of $Zn(Ac)_2$, which was first heated at 400 °C for different times and then heated to 600 °C for 12 h. (a, b) 1 h, (c, d) 3 h, and (e, f) 6 h.

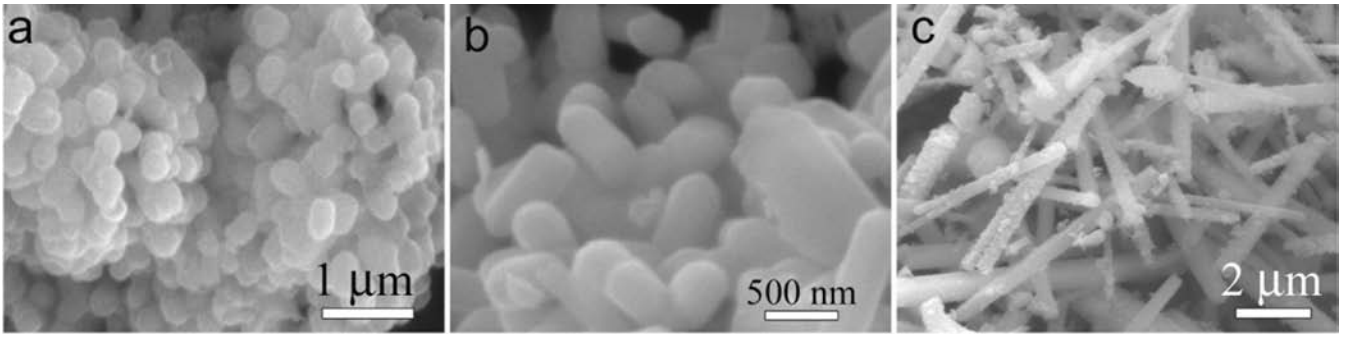

Figure 8. SEM images of the as-obtained $ZnCO_3$ nanostructures prepared by ethanol-assisted thermolysis of $Zn(Ac)_2$ at a temperature of 400 °C for different reaction times: (a) 3 h, (b) 6 h, and (c) 12 h.

fractions (Figure S5, Supporting Information). Figure S5a shows the photographic images of the liquid fractions obtained from the thermolysis of $Zn(Ac)_2$ in the presence of ethanol at temperatures of 200, 300, and 400 °C for 12 h, which are denoted as L-200, L-300, and L-400, respectively. The deepening color indicates the increase of the polymerization degree of ethanol and the content of the oligomers in the liquid fractions with the increase of reaction temperature. A large number of organic compounds in the liquid fractions are detected by GC−MS analysis in

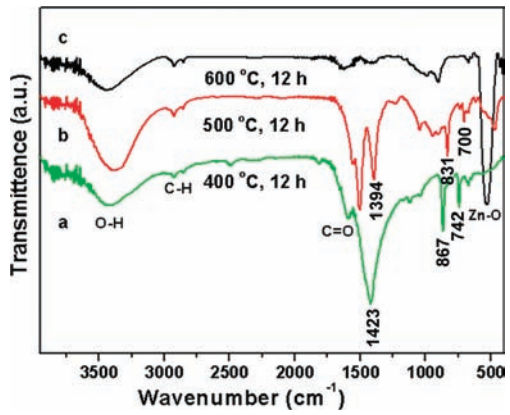

Figure 9. FT-IR spectra of the as-obtained samples prepared by ethanol-assisted thermolysis of $Zn(Ac)_2$ at different temperatures for 12 h: (a) 400 °C, (b) 500 °C, and (c) 600 °C.

this work. All of the typical components found by GC−MS can be divided into aromatic and nonaromatic compounds (Figure S6, Supporting Information). The aromatic compounds undoubtedly originated from the aromatic cyclodehydration of ethanol.

In our recent work, it was found that the oligomers produced by polymerization of ethanol act as structure-directing agents by selective adsorption to induce the self-assembly of carbon colloidal spheres to form novel spheroidal carbons.[21] In this work, these oligomers including aromatic and nonaromatic compounds act as structure-directing agents to direct the growth of $ZnCO_3$ nanostructures by means of selective adsorption on certain crystal faces to hinder the growth of the crystal and affect its final morphology. FT-IR spectroscopy provides the evidence to support the presence of oligomer adsorption on the surface of $ZnCO_3$ nanoparticles (Figure 9). It reveals that, in all three samples, the strong characteristic peak at 3420 cm^{-1} is attributed to the O−H stretching vibration, which may be from the absorbed hydroxyl groups or water. The absorption peak at 1120 cm^{-1} corresponds to the C−OH stretching and OH bending vibrations, and the peaks at 2927 and 2850 cm^{-1} originate from the C−H stretching vibration. The weak peaks in the 1000−1450 cm^{-1} range correspond to C−O (hydroxyl, ester, or ether) stretching and O−H bending vibrations. Two sharp vibration bands centered at 867 and 742 cm^{-1}, together with a broad absorbance band centered at 1423 cm^{-1}, are the characteristic FT-IR bands of $ZnCO_3$ (Figure 9a). The vibration bands for C−O stretching that are normally observed at 1463.4 and 875.7 cm^{-1} for CO_3^{2-} shift down to 1423 and 867 cm^{-1}, respectively, in the present case.[22] This shift can also be observed when compared with the normal locations from the bulk of the zinc carbonate base, for which the normal absorption peaks of CO_3^{2-} are located at about 1438 and 871 cm^{-1} (Figure S7, Supporting Information). This shift results from the vibration motion of CO_3^{2-}, which is restricted by the selective adsorption of organic groups such as hydroxyl and carboxyl. When the temperature reaches 500 °C, all three vibration bands of $ZnCO_3$ remained, whereas their intensities decreased (Figure 9b), indicating that the $ZnCO_3$ phase still exists in the sample treated at 500 °C, which is in excellent agreement with the XRD results. Interestingly, the peaks of CO_3^{2-} shift down to 1394 and 831 cm^{-1}, which is more prominent than that of the 400 °C treated sample, and the other characteristic peak of $ZnCO_3$ at about 742 cm^{-1} is also shifted down to 700 cm^{-1}, indicating that $ZnCO_3$ nanoparticles were encapsulated by oligomers (Figure 9b). As shown in Figure 9c, the newly developed peak at about 529 cm^{-1} arises from the stretching vibration of Zn−O bond. The peaks at 1423, 867, and 742 cm^{-1} of $ZnCO_3$ cannot be distinguished, indicating the complete decomposition of $ZnCO_3$. Another noticeable change in this sample is, as shown in Figure 9c, is that the band centered at about 1500 cm^{-1} originating from the benzene ring framework vibrations of certain aromatic compounds disappeared, suggesting the carbonization of the oligomers. These results indicate that ZnO nanostructures, as well as $ZnCO_3$ nanoparticles, are absorbed by the oligomers and highly functionalized with organic groups including hydroxyl and carboxyl groups. In addition, the oligomers act as carbon precursors to result in carbon encapsulation as well as structure-directing agents. With increasing reaction temperature, the in-situ carbonization of these oligomers on the surface of the ZnO nanostructures results in the formation of ZnO@C core/shell structures and final carbon hollow structures after HCl etching.

From the above evidence and analysis, it can be concluded that these novel carbon hollow structures are formed from the in-situ templates of ZnO nanoparticles that are produced by the decomposition of $ZnCO_3$ nanostructures resulting from the pyrolysis of $Zn(AC)_2$ initially, and the in-situ carbonization of the oligomers results in the fabrication of ZnO@C core/shell structures. This in-situ template technique has several advantages over conventional template strategies. First, this template is generated in situ, which makes the presynthesis of the templates unnecessary. Moreover, the in-situ template is highly functionalized and selectively absorbed with organic groups, which results in the uniform coating of the carbon precursor over the template surfaces, and thus carbon hollow structures with relatively uniform particle size and shell thickness can be achieved. More importantly, the controlled synthesis of the carbon hollow structures can be realized easily by tuning the morphology of the $ZnCO_3$ nanostructures via controlling the reaction time and the thermolysis procedure.

Formation Mechanism of the Carbon Hollow Structures. Based on all the results above, the formation mechanism of these carbon hollow structures is proposed and schematically shown in Figure 10. In the first step, $ZnCO_3$ nanoparticles are generated followed by self-assembly and growth into spherical nanostructures. In the meantime, polymerization of ethanol leads to the generation of oligomers, which are absorbed on the surface of $ZnCO_3$ nanoparticles. The in-situ carbonization of oligomers results in the formation of carbon encapsulations when the temperature increases to 500 °C and above. Meanwhile, the $ZnCO_3$ nanoparticles are decomposed in situ to form ZnO nanostructures; thus, the ZnO@C core/shell structures are obtained (step 2). In the third step, the

(21) Zheng, M.; Liu, Y.; Jiang, K.; Xiao, Y.; Yuan, D. *Carbon* **2010**, *48*, 1224–1233.
(22) White, W. B. In *Infrared Spectra of Minerals*; Farmer, V. C., Ed.; Mineralogical Society: London, 1974; pp 227−284.

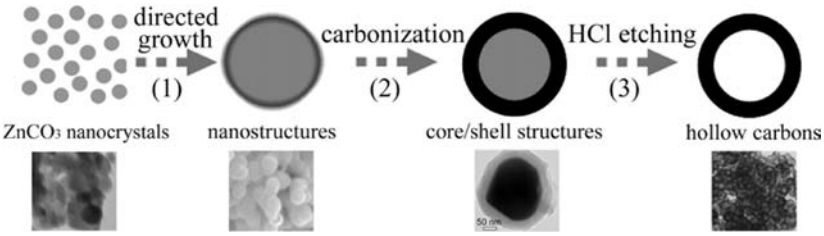

Figure 10. Schematic representation of the possible formation mechanism of the carbon hollow structures by ethanol-assisted thermolysis of $Zn(Ac)_2$.

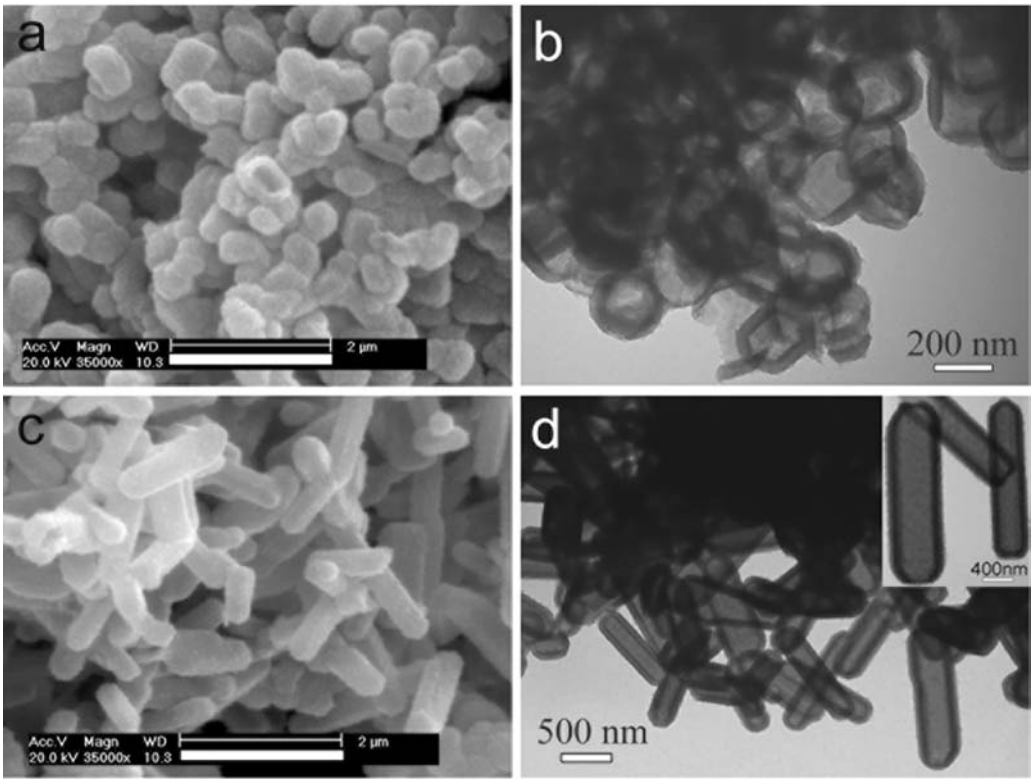

Figure 11. SEM and TEM images of the products calcined at 1200 °C for 6 h: (a, b) nanocapsules and (c, d) hollow nanorods. Scale bars of a and c: 2 μm.

removal of the ZnO cores by HCl etching results in the formation of carbon hollow structures.

Obviously, the directed growth of $ZnCO_3$ nanoparticles is the critical step for the controlled synthesis of carbon hollow structures. The oligomers generated in the early stage of the thermolysis act as structure-directing agents by absorbing onto certain exposed surfaces of $ZnCO_3$ nanoparticles to hinder their growth, while those surfaces that are not hindered will preferentially develop. Maintaining the temperature at 400 °C for different times, $ZnCO_3$ nanostructures with different aspect ratios are formed; subsequently, the in-situ carbonization leads to the formation of ZnO@C core/shell structures with different morphologies. After etching by HCl, carbon hollow structures, such as nanospheres, nanocapsules, nanorods, and microtubes, can be acquired.

Thermal Stability of the Carbon Hollow Structures. It is known that, in the synthesis of hollow metal and other inorganic materials, the removal of the core structures by etching or calcination usually leads to a certain degree of damage to the shell structure. Usually, the obtained hollow structures exhibit poor thermal stability, and the collapse of the structure is a common phenomenon especially under high-temperature conditions.[23] We measured the thermal stability of synthesized carbon hollow structures, which was performed by calcination at 1200 °C for 6 h under a nitrogen atmosphere. Figure 11 shows the SEM and TEM images of the calcinated nanocapsules and hollow nanorods. No collapse of the hollow structures is observed, indicating these carbon hollow structures exhibit excellent thermal and structural stability. Furthermore, the HRTEM images show the presence of graphitic layers in the shell, suggesting the improvement of graphitization degree of these hollow carbons (Figure S8, Supporting Information). Figure S9 shows the XRD patterns of the uncalcined and calcined samples. It can be observed that the intensity of the two diffraction peaks of (002) and (10) increased, also indicating the improvement of the graphitization of the calcined samples. Owing to their excellent thermal and structural

(23) (a) Zhang, D.; Yang, D.; Zhang, H.; Lu, C.; Qi, L. *Chem. Mater.* **2006**, *18*, 3477–3485. (b) Wang, X.; Xiao, P. *J. Mater. Res.* **2005**, *20*, 796–800. (c) Guo, C.; Cao, Y.; Xie, S.; Dai, W.; Fan, K. *Chem. Commun.* **2003**, *7*, 700–701. (d) Wong, M.; Cha, J.; Choi, K. S.; Deming, T. J.; Stucky, G. D. *Nano Lett.* **2002**, *2*, 583–587.

stability, both the calcined and uncalcined carbon hollow structures can be used in catalyst supports in harsh conditions and other advanced applications.

Conclusion

In conclusion, we have developed a simple in-situ template method to fabricate carbon hollow structures by the controlled thermolysis of $Zn(Ac)_2$ in the presence of ethanol. The carbon hollow spheres, nanocapsules, nanorods, and microtubes can be obtained by this method. The particle size, shell thickness, and morphology of the carbon hollow structures highly depend on the heating process employed. When the samples are directly prepared at 600 °C for different reaction times from 3 to 48 h, carbon nanocapsules with shell thicknesses from 15 to 70 nm are obtained, and the cavity size increases from 80 to 600 nm with the increase of reaction time. When the samples are first heated at 400 °C for different times from 1 to 6 h and then heated to 600 °C for 12 h, we can obtain carbon capsules with different morphologies and aspect ratios. For instance, in a short reaction time of 1 h at 400 °C, carbon nanocapsules with an aspect ratio of about 1.5 are obtained. As the reaction time increases to 2−3 h, hollow nanorods with an aspect ratio of about 3.0 can be achieved. Extending the thermolysis time to 6 h, micrometer-sized carbon tubes are formed. On the basis of our results, the growth process and mechanism of the carbon hollow structures are proposed. Furthermore, the obtained carbon hollow structures show excellent thermal stability, which may lead to new applications in many fields. These carbon hollow structures may have broad application prospects in catalysis support, drug delivery, hydrogen storage, adsorption, and so on.[3−7] This work may also open up new opportunities for the controlled synthesis of the metal oxides (or metals)/C core/shell structures and carbon hollow structures by the thermolysis process of metal organic compounds in an appropriate organic solvent.

Acknowledgment. This work was supported by the National Natural Science Found of China (Grant Nos. U0734005 and 20906037) and the Fundamental Research Funds for the Central Universities (No. 21610102).

Supporting Information Available: SEM images of the broken nanospheres, TEM images of the ZnO/C core/shell structures with different shapes and aspect ratios, SEM images of carbon aggregates, GC−MS and typical components of the liquid fractions, and TEM images of calcined carbon hollow structures. This material is available free of charge via the Internet at http://pubs.acs.org.